Measurements of Ion Stopping Around the Bragg Peak in High-Energy-Density Plasmas

J. A. Frenje,[1] P. E. Grabowski,[2] C. K. Li,[1] F. H. Séguin,[1] A. B. Zylstra,[1,*] M. Gatu Johnson,[1] R. D. Petrasso,[1] V. Yu Glebov,[3] and T. C. Sangster[3]

[1]*Plasma Science and Fusion Center, Massachusetts Institute of Technology, Cambridge, Massachusetts 02139, USA*
[2]*Department of Chemistry, University of California Irvine, Irvine, California 92697, USA*
[3]*Laboratory for Laser Energetics, University of Rochester, Rochester, New York 14623, USA*

(Received 14 April 2015; published 9 November 2015)

For the first time, quantitative measurements of ion stopping at energies around the Bragg peak (or peak ion stopping, which occurs at an ion velocity comparable to the average thermal electron velocity), and its dependence on electron temperature (T_e) and electron number density (n_e) in the range of 0.5–4.0 keV and 3×10^{22} to 3×10^{23} cm^{-3} have been conducted, respectively. It is experimentally demonstrated that the position and amplitude of the Bragg peak varies strongly with T_e with n_e. The importance of including quantum diffraction is also demonstrated in the stopping-power modeling of high-energy-density plasmas.

DOI: 10.1103/PhysRevLett.115.205001 PACS numbers: 52.25.Fi, 52.38.Ph, 52.70.Nc

A fundamental understanding of DT-alpha stopping in high-energy-density plasmas (HEDP) is essential to achieving hot-spot ignition at the National Ignition Facility (NIF) [1]. This requires accurate knowledge about the evolution of plasma conditions and the DT-alpha transport and energy deposition in plasmas for a wide range of electron (T_e) and ion temperatures (T_i) spanning from tens of eV to tens of keV, and electron number densities (n_e) from $\sim10^{21}$ to $\sim10^{26}$ cm^{-3}.

Over the last decades, ion stopping in weakly coupled to strongly coupled HEDP has been subject to extensive analytical and numerical studies [2–10], but only a limited set of experimental data exists to validate these theories. Most previous experiments also used only one type of ion with relatively high initial energy, in plasmas with $n_e < 10^{23}$ cm^{-3} and $T_e < 60$ eV [11–21]. In addition, none of these experiments probed the detailed characteristics of the Bragg peak (or peak ion stopping), which occurs at an ion velocity comparable to the average thermal electron velocity. To the best of our knowledge, only one experimental attempt to do this was made by Hicks *et al.* [22], who measured ion stopping in a plasma with T_i of ~5 keV and n_e of $\sim10^{22}$ cm^{-3}. In this experiment, Hicks *et al.* measured energy loss of the ions produced in the nuclear reactions

$$\mathrm{D}+\mathrm{D}\rightarrow t(1.01\ \mathrm{MeV})+p(3.02\ \mathrm{MeV}), \tag{1}$$

$$\mathrm{D}+{}^{3}\mathrm{He}\rightarrow {}^{4}\mathrm{He}(3.71\ \mathrm{MeV})+p(14.63\ \mathrm{MeV}), \tag{2}$$

where the birth energies shown in the parentheses are for a "zero temperature" plasma [23]. From the observed energy losses of these ions, Hicks *et al.* were able to describe qualitatively the behavior of the ion stopping for one plasma condition. The work described here makes significant advances over previous experimental efforts, by quantitatively assessing the characteristics of the ion stopping around the Bragg peak for different HEDP conditions. This was done through accurate measurements of energy loss of the four ions, produced in reactions (1) and (2).

The new experiment, carried out at the OMEGA laser [24], involved implosions of eighteen thin SiO_2 capsules filled with equimolar deuterium-^{3}He gas. The capsule shells were 850 to 950 μm in diameter, 2.1 to 2.8 μm thick, and had an initial gas-fill pressure ranging from 3 to 27 atm. These capsules were imploded with sixty laser beams that uniformly delivered up to 10.6 kJ to the capsule in a 0.6-ns or 1-ns square pulse, resulting in a laser intensity on capsule up to $\sim4\times10^{14}$ W/cm^2 [25]. Table I lists the capsule and laser parameters, along with some measured and inferred implosion parameters for a subset of four implosions discussed in detail in this Letter.

To determine the energy lost by the four ions as they traversed the plasma, energy spectra of the emitted ions were measured simultaneously with two magnet-based charged-particle spectrometers (CPS1 and CPS2) [28]. Six wedge-range-filter proton spectrometers [28] positioned at various locations around the implosion were also used to measure D^{3}He-proton spectrum. An example of spectra measured with CPS2 for two implosions, with similar total areal-density (ρR) values [29], where most of the energy loss took place in the cold remaining glass shell (blue spectra) and in the hot D^{3}He fuel (red spectra) is shown in Fig. 1. By contrasting the measured mean energies, indicated in Fig. 1, to the birth energies of the ions (temperature corrected), an average energy loss ($-\Delta E_i$) was determined and used to assess the plasma stopping power. As shown in Fig. 1, the DD tritons, DD protons, and D^{3}He alphas display significantly larger $-\Delta E_i$ in the cold plasma than in the hot plasma. The D^{3}He protons, on the other hand, exhibit a similar $-\Delta E_i$ in these two plasmas, as they probe plasma stopping at velocities

TABLE I. Capsule and laser parameters for four selected implosions, and measured DD burned-averaged T_i and determined key implosion parameters [n_i, T_e, n_e ($n_e \approx 1.5 n_i$), plasma-coupling parameter (Γ), degeneracy parameter (θ) [27] and total ρR, for the region where the energy loss mainly occurred]. For implosion 29828, the energy loss took place mainly in the colder glass-shell plasma, while for the other implosions, the energy loss took place mainly in the hotter D^3He plasma.

Shot	Capsule	Laser pulse	Laser energy [kJ]	T_i [keV]	n_i [cm^{-3}]	T_e [keV]	n_e [cm^{-3}]	Γ [%]	θ	Total ρR [mg/cm^2]
27814	D^3He(18 atm)SiO_2[2.3 μm]OD[948 μm]	1-ns square	8.4	3.7	2×10^{23}	1.8	3×10^{23}	0.9	110	8.1
29828	D^3He(18 atm)SiO_2[2.6 μm]OD[917 μm]	0.4-ns Gaussian	9.4	6.7	3×10^{22}	0.6	5×10^{22}	1.4	120	2.0
43233	D^3He(18 atm)SiO_2[2.5 μm]OD[855 μm]	1-ns square	10.6	11.6	5×10^{22}	3.9	8×10^{22}	0.3	580	3.5
43235	D^3He(18 atm)SiO_2[2.5 μm]OD[854 μm]	1-ns square	9.9	10.1	2×10^{22}	2.1	3×10^{22}	0.3	600	1.4

well above the Bragg peak. These differences are discussed in detail below. In addition, the uncertainties associated with the measured mean energies shown in Fig. 1, are mainly due to the spectrometer energy-calibration error (in some cases statistics also affects the uncertainties), which dictates the total uncertainty in the determined $-\Delta E_i$.

To make use of the measured $-\Delta E_i$ and assess the plasma stopping power, it is necessary to determine the HEDP conditions through which the ions traversed. For each implosion, a T_i and a DD yield were measured from the Doppler broadened neutron-time-of-flight signal [30]. A second measurement of T_i was obtained for each implosion from the DD-D^3He yield ratio, and the T_i values and uncertainties used in this Letter are weighted averages of these two measurements. D^3He and DD burn profiles were measured with the proton core imaging system [31], and the D^3He and DD burn duration was measured with the

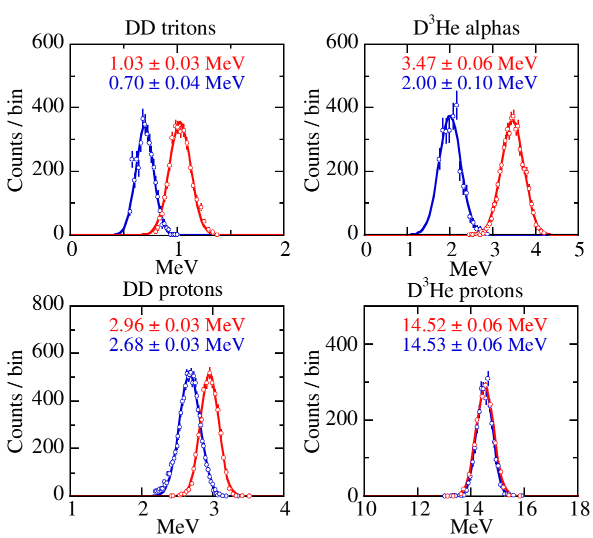

FIG. 1 (color online). CPS2-measued spectra of DD tritons, D^3He alphas, DD protons, and D^3He protons produced in implosions 29828 (blue) and 43233 (red). These experiments were designed to generate similar total ρR values but to have most of the ion energy loss taking place in the cold remaining shell for implosion 29828 (blue spectra) and in the hot fuel for implosion 43233 (red spectra).

particle temporal diagnostic and neutron temporal diagnostic (NTD) [32,33], respectively. A secondary-neutron yield relative to the primary neutron yield (Y_{2n}/Y_{1n}) was also measured for a D^3He-fuel ρR determination [34].

For the eighteen implosions, the measured DD and D^3He yield ranged from 2.0×10^9 to 1.2×10^{10} and from 1.2×10^8 to 1.3×10^{10}, respectively; T_i ranged from 2.7 to 11.6 keV; the DD- and D^3He-burn duration both ranged from 150 to 180 ps; and the measured size of the DD- and D^3He-burn profiles ranged from ~45 to ~100 μm and ~30 to ~60 μm (radius at $1/e$ relative to the peak intensity), respectively. Using 1D modeling of the implosion, involving a parabolic temperature profile and constant D^3He-fuel density, a good match to these nuclear observables was found for average ion-number densities (n_i) ranging of 2×10^{22} to 2×10^{23} cm^{-3} ($n_e \approx 1.5 n_i$ for these D^3He plasmas). T_e could not be measured directly in these experiments, but was qualitatively and independently assessed from the n_e, n_i, T_i, and burn-duration data. A Y_{2n}/Y_{1n} ratio up to $(3.96 \pm 0.17)\times10^{-4}$ was measured, which corresponds to a D^3He fuel ρR up to 7 mg/cm^2. The ρR of the remaining unablated shell was determined from benchmarked 1D simulations [35], which indicate that the fuel ρR is about an order of magnitude larger than the remaining-shell ρR for the implosions with a 1-ns laser-pulse drive, while the remaining-shell ρR dominates the D^3He-fuel ρR for the implosions with a 0.4-ns laser pulse. As a consequence, the ion energy loss is mainly taking place in the D^3He fuel in the 1-ns implosions and in the remaining unablated shell in the 0.4-ns implosions.

Although the HEDP conditions have been characterized, the information is not sufficient for distinguishing state-of-the-art plasma-stopping-power theories at $v_i \sim v_{\rm th}$, i.e., at the Bragg peak, which is the long-term goal of this effort. For this, we need information on how the spatial profiles of n_e and T_e vary in time during the nuclear production period. Instead, our aim is twofold. First, we simply aim to experimentally demonstrate that the amplitude of the position and amplitude of the Bragg peak varies strongly with T_e with n_e. Second, as the impact parameter of the closest approach between the projectile ions and plasma electrons can be smaller than the de Broglie wavelength, we also aim to demonstrate the importance of including quantum diffraction in the stopping-power modeling of the ion energy loss at these HEDP conditions.

The Brown-Preston-Singleton (BPS) [4] and the Li-Petrasso (LP) stopping [5] formalisms were used to model the data. The BPS formalism includes a Coulomb logarithm in the weakly coupled limit, which is derived using the dimensional continuation method, and the LP stopping formalism is derived from a Fokker-Planck collision operator that uses an *ad hoc* Coulomb logarithm. Although these formalisms have limitations, they are used in this work to explore if the dominant physics is captured. Figure 2 illustrates the BPS (black solid) and LP (green solid) proton stopping curves, given in $\mathrm{keV}/(\mathrm{mg}/\mathrm{cm}^2)$, for a hypothetical uniform plasma that is representative for the HEDP conditions in these experiments. At $v_i > v_{\mathrm{th}}$, the BPS and LP formalisms predict similar charged-particle stopping, while there is ~20% at $v_i \sim v_{\mathrm{th}}$. The BPS quantum (dotted black) and the BPS classical (dashed black) are also shown to illustrate their significance. For this plasma condition, the quantum reduction to the classical ion stopping is ~25%–30%.

An effective way to evaluate the measured $-\Delta E_i$ of ions with different birth energy (E_i), charge (Z_i), and mass (A_i) is to show the dependency between $-\Delta E_i/Z_i^2$ and E_i/A_i. Presenting the data in this form, the ion energy loss is almost exclusively a function of v_i (any explicit dependence on A_i and Z_i is small and restricted to the slowly varying Coulomb logarithm) and can easily be analyzed using a plasma stopping-power model. Figures 3(a) and 3(b) illustrate the $-\Delta E_i/Z_i^2$ vs E_i/A_i dependence on T_e. This data set was directly determined from the low-temperature and high-temperature data shown in Fig. 1. The black (green) curves are the BPS (LP) modeled fits to the data. These curves were obtained by integrating the plasma-stopping-power functions over assumed values of T_e and ρR, which were varied until best fits to the data were obtained. Clearly, these experimental results demonstrate that the plasma-stopping-power function varies with T_e in the framework of the BPS and LP formalisms. At T_e of ~0.6 keV ($\Gamma = 1.4\%$; see Table I), the effective proton Bragg peak is $220\ \mathrm{keV}/(\mathrm{mg}/\mathrm{cm}^2)$, which is reduced to 40 keV per $\mathrm{mg}/\mathrm{cm}^2$ for a T_e of ~4 keV ($\Gamma = 0.3\%$; see Table I). This reduction is caused by the fact that $v_i \sim v_{\mathrm{th}}$ for the DD tritons, D^3He alphas, and DD protons in the low-temperature case, while $v_i < v_{\mathrm{th}}$ for these ions in the high-temperature case. This agrees with theories in which the Bragg peak scales with $1/T_e$. The average energy loss of the D^3He protons is, on the other hand, unaffected by an increasing T_e because $v_i > v_{\mathrm{th}}$. In contrast, the two data sets shown in Figs. 4(a) and 4(b) illustrate the $-\Delta E_i/Z_i^2$ vs E_i/A_i dependence on ρR (or n_e [29]), which indicates that the D^3He-proton energy loss increases with increasing ρR with ~$40\ \mathrm{keV}/(\mathrm{mg}/\mathrm{cm}^2)$.

To fully constrain and validate the stopping-power formalisms used to model this type of data, an independent measurement of T_e and ρR (or n_e) must be made. In these experiments, T_e could not be measured directly, but a D^3He fuel ρR was determined from the measured Y_{2n}/Y_{1n} ratio for most implosions. In the case of the high-ρR implosion shown in Fig. 4(b) (implosion 27814), a Y_{2n}/Y_{1n} ratio of $(3.96 \pm 0.17) \times 10^{-4}$ was measured, which corresponds to a D^3He-fuel ρR of $7.1 \pm 0.3\ \mathrm{mg}/\mathrm{cm}^2$. According to benchmarked 1D-implosion simulations, this represents 88% of the total ρR of $8.1 \pm 0.3\ \mathrm{mg}/\mathrm{cm}^2$ (D^3He fuel ρR + glass shell ρR). Figure 5 shows the high-ρR implosion data contrasted to BPS and LP modeling that uses the fixed ρR value of $8.1\ \mathrm{mg}/\mathrm{cm}^2$ and a varying T_e to minimize the reduced χ^2. For comparison, BPS modeling of the data was also done when the quantum component was switched off. Here, the inferred T_e is dictated mainly by the energy loss

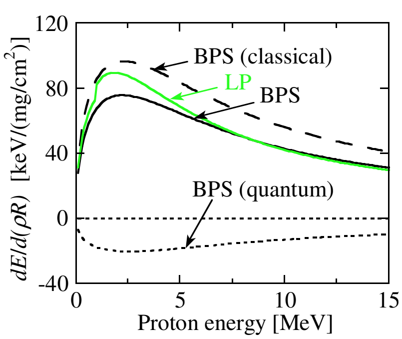

FIG. 2 (color online). Brown-Preston-Singleton (BPS) and Li-Petrasso (LP) modeling of proton stopping in a uniform plasma with a T_e of 1.0 keV and n_e of $5 \times 10^{22}\ \mathrm{cm}^{-3}$. The BPS quantum (dotted black) and BPS classical stopping (dashed black) are also shown.

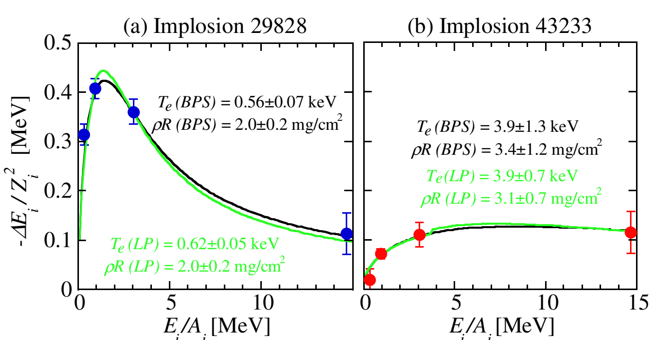

FIG. 3 (color online). Stopping-power data illustrating T_e dependence. Measured and modeled $-\Delta E_i/Z_i^2$ versus E_i/A for a low-temperature experiment (a), and for a high-temperature experiment (b). Inferred ρR was similar in these experiments. The data were determined directly from the spectra shown in Fig. 1. The black (green) curves represent the BPS (LP) modeling. For the low-temperature experiment, the reduced χ^2 [36] is 2.1 for LP and 0.2 for BPS, and for the high-temperature experiment, the reduced χ^2 is 1.5 for LP and 1.5 for BPS. The errors on the inferred T_e and ρR values were determined from the reduced χ^2 fit.

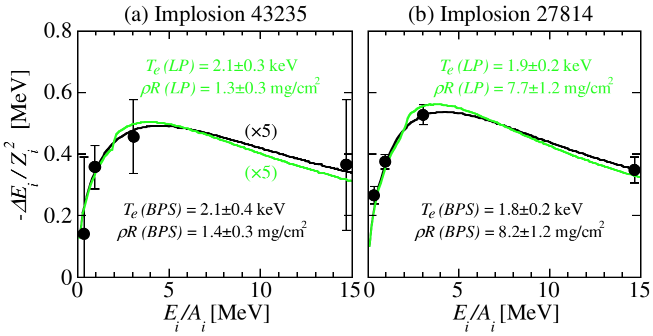

FIG. 4 (color online). Stopping-power data illustrating ρR (or n_e) dependence. Measured and modeled $-\Delta E_i/Z_i^2$ versus E_i/A for a low-ρR experiment ($n_e \sim 3\times10^{22}$ cm^{-3}) (a), and for a high-ρR experiment ($n_e \sim 3\times10^{23}$ cm^{-3}) (b). The experimental and modeled data shown in (a) have been multiplied with a factor of 5 to put the information on the same scale as used in (b). Inferred T_e was similar in these experiments. The black (green) curves represent the BPS (LP) modeling. For the low-ρR experiment, the reduced χ^2 is 0.4 for LP and 0.2 for BPS, and for the high-ρR experiment, the reduced χ^2 is 2.3 for LP and 0.7 for BPS. The errors on the inferred T_e and ρR values were determined from the reduced χ^2 fit.

of the DD tritons, D^{3}He alphas, and DD protons because $v_{\rm th}$ is similar to the velocities of these ions. In contrast, the energy loss of the D^{3}He-protons is insensitive to T_e for these plasma conditions, but linearly proportional to the ρR. As a consequence, the classical modeling can be shown to be experimentally inconsistent with the ρR measurement and its uncertainty alone. We find that classical BPS theory overpredicts the ion stopping, indicating the importance of including quantum diffraction in the plasma-stopping-power modeling of the energy-loss data in these weakly coupled HEDP. In addition, the full BPS and LP formalisms agree with the data for $v_i > v_{\rm th}$, while there are some discrepancies for $v_i \sim v_{th}$. However, as the plasma stopping power at $v_i \sim v_{\rm th}$ is highly sensitive to T_e, and that a direct measurement of T_e is lacking, any definite conclusions about the modeling of the data at $v_i \sim v_{\rm th}$ cannot be made with this data set. To further validate and elucidate stopping-power formalisms at the Bragg peak, measurements of $n_e(r,t)$ and $T_e(r,t)$ will be conducted in future experiments using x-ray imaging spectroscopy of a dopant such as argon in the D^{3}He fuel [37].

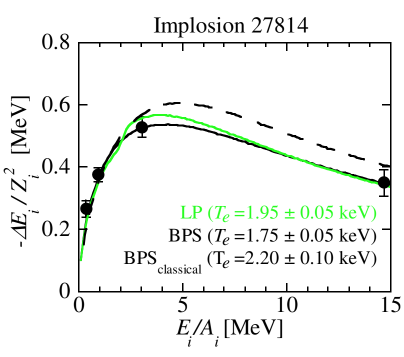

FIG. 5 (color online). Measured and modeled $-\Delta E_i/Z_i^2$ versus E_i/A for implosion 27814. In the modeling of the energy-loss data, ρR was fixed to 8.1 mg/cm^2 while T_e was allowed to vary. The reduced χ^2 is 10.1 for BPS-classical (dashed black), 0.7 for BPS (solid black) and 1.7 for LP (solid green). The errors on the inferred T_e values were determined from the reduced χ^2 fit.

In summary, ion stopping around the Bragg peak and its dependence on plasma conditions has been measured for the first time in HEDP. The experimental data generally support the predictions of the BPS and LP formalisms, demonstrating the plasma stopping-power variation with T_e and ρR (or n_e). It has also been experimentally demonstrated that classical stopping overpredicts the ion stopping, which is to be expected as it does not include quantum diffraction. The BPS and LP formalisms, with 25%–30% quantum reduction to the ion stopping, agree with the data for $v_i > v_{\rm th}$. There are some differences at $v_i \sim v_{\rm th}$, but the current data set cannot distinguish between them. These experimental results represent the first sensitive tests of plasma-stopping-power theories around the Bragg peak, an important first step towards accurately validating state-of-the-art plasma-stopping-power theories, which use microscopically based quantum approaches that overcome the limitations of the BPS and LP models used in this work. In addition, the long-term goal with this effort is to establish a fundamental understanding of DT-alpha stopping in HEDP, which is a prerequisite for achieving hot-spot ignition at the NIF.

The work described herein was performed in part at the LLE National Laser User's Facility (NLUF), and was supported in part by U.S. DOE (Grant No. DE-FG03-03SF22691), LLNL (subcontract Grant No. B504974), and LLE (subcontract Grant No. 412160-001G). In addition, P. E. G. acknowledges support from the Laboratory Directed Research and Development Program at LLNL under tracking code No. 12-SI-005.

*Present address: Los Alamos National Laboratory, Los Alamos, New Mexico 87545, USA.

[1] G. H. Miller, E. I. Moses, and C. R. Wuest, The National Ignition Facility: Enabling fusion ignition for the 21st century, Nucl. Fusion **44**, S228 (2004).
[2] T. A. Mehlhorn, A finite material temperature model for ion energy deposition in ion driven inertial confinement fusion targets, J. Appl. Phys. **52**, 6522 (1981).
[3] T. Peter, and J. Meyer-ter-Vehn, Energy loss of heavy ions in dense plasma. I. Linear and nonlinear Vlasov theory for the stopping power, Phys. Rev. A **43**, 1998 (1991).
[4] L. S. Brown, D. Preston, and R. Singleton Jr., Charged particle motion in a highly ionized plasma, Phys. Rep. **410**, 237 (2005).
[5] C. K. Li and R. D. Petrasso, Charged-Particle Stopping Powers in Inertial Confinement Fusion Plasmas, Phys. Rev. Lett. **70**, 3059 (1993); **114**, 199901(E) (2015).

[6] D. O. Gericke, M. Schlanges, and W. D. Kraeft, Stopping power of a quantum plasma—T-matrix approximation and dynamical screening, Phys. Lett. A **222**, 241 (1996).

[7] G. Zwicknagel, C. Toepffer, and P.-G. Reinhard, Stopping of heavy ions in plasmas at strong coupling, Phys. Rep. **309**, 117 (1999).

[8] G. Maynard, and C. Deutsch, Energy loss and straggling of ions with any velocity in dense plasmas at any temperature, Phys. Rev. A **26**, 665 (1982).

[9] G. Maynard, and C. Deutsch, Born random phase approximation for ion stopping in an arbitrarily degenerate electron fluid, J. Phys. (Paris) **46**, 1113 (1985).

[10] P. E. Grabowski, M. P. Surh, D. F. Richards, F. R. Graziani, and M. S. Murillo, Molecular Dynamics Simulations of Classical Stopping Power, Phys. Rev. Lett. **111**, 215002 (2013).

[11] F. C. Young, D. Mosher, S. J. Stephanakis, S. A. Goldstein, and T. A. Mehlhorn, Measurements of Enhanced Stopping of 1-MeV Deuterons in Target-Ablation Plasmas, Phys. Rev. Lett. **49**, 549 (1982).

[12] D. H. H. Hoffmann, K. Weyrich, H. Wahl, D. Gardés, R. Bimbot, and C. Fleurier, Energy loss of heavy ions in a plasma target, Phys. Rev. A **42**, 2313 (1990).

[13] G. Belyaev *et al.*, Measurement of the Coulomb energy loss by fast protons in a plasma target, Phys. Rev. E **53**, 2701 (1996).

[14] C. Stöckl *et al.*, Experiments on the interaction of heavy-ion beams with dense plasmas, Fusion Sci. Tech. **31**, 169 (1997).

[15] C. Stöckl *et al.*, Experiments on the interaction of ions with dense plasma at GSI-Darmstadt, Nucl. Instrum. Methods Phys. Res., Sect. A **415**, 558 (1998).

[16] M. Roth, C. Stöckl, W. Süß, O. Iwase, D. O. Gericke, R. Bock, D. H. H. Hoffmann, M. Geissel, and W. Seelig, Energy loss of heavy ions in laser-produced plasmas, Europhys. Lett. **50**, 28 (2000).

[17] A. Golubev *et al.*, Experimental investigation of the effective charge state of ions in beam-plasma interaction, Nucl. Instrum. Methods Phys. Res., Sect. A **464**, 247 (2001).

[18] K. Shibata, A. Sakumi, R. Sato, K. Tsubuku, J. Hasegawa, M. Ogawa, and Y. Oguri, A TOF system to measure the energy loss of low energy ions in a hot dense plasma, Nucl. Instrum. Methods Phys. Res., Sect. B **161**, 106 (2000).

[19] A. B. Zylstra *et al.*, Measurement of Charged-Particle Stopping in Warm Dense Plasma, Phys. Rev. Lett. **114**, 215002 (2015).

[20] F. R. Graziani *et al.*, Large-scale molecular dynamics simulations of dense plasmas: The Cimarron Project, High Energy Density Phys. **8**, 105 (2012).

[21] J. Jacoby *et al.*, Stopping of Heavy Ions in a Hydrogen Plasma, Phys. Rev. Lett. **74**, 1550 (1995).

[22] D. G. Hicks *et al.*, Charged-particle acceleration and energy loss in laser-produced plasmas, Phys. Plasmas **7**, 5106 (2000).

[23] For a finite temperature, the mean energy of the fusion products is slightly upshifted by a few tens of keV [22].

[24] T. R. Boehly *et al.*, Initial performance results of the OMEGA laser system, Opt. Commun. **133**, 495 (1997).

[25] For these laser and capsule conditions, it has been demonstrated that capsule charging and any energy upshifts of the produced ions are insignificant and thus have no impact on these energy-loss measurements [26]. This is critical when equating a measured energy loss to plasma stopping.

[26] N. Sinenian, M. J.-E. Manuel, J. A. Frenje, F. H. Séguin, C. K. Li, and R. D. Petrasso, An empirical target discharging model relevant to hot-electron preheat in direct-drive implosions on OMEGA, Plasma Phys. Controlled Fusion **55**, 045001 (2013).

[27] For the plasma degeneracy parameter (θ) shown in Table I, we used the standard definition of $k_B T_e / E_F$, where k_B is the Boltzmann's constant and E_F is the Fermi energy.

[28] F. H. Séguin *et al.*, Spectrometry of charged particle from inertial-confinement-fusion plasmas, Rev. Sci. Instrum. **74**, 975 (2003).

[29] For these low-convergence implosions, which are 1D in nature, the ion-number density (n_i) in the D^3He fuel scales with ρR as $n_i \sim \rho R^{1.5}$. This means that the electron number density in the clean D^3He fuel scales with ρR as $n_e \sim 1.5 \rho R^{1.5}$.

[30] V. Yu. Glebov, C. Stoeckl, T. C. Sangster, S. Roberts, G. J. Schmid, R. A. Lerche, and M. J. Moran, Prototypes of National Ignition Facility neutron time-of-flight detectors tested on OMEGA, Rev. Sci. Instrum. **75**, 3559 (2004).

[31] F. H. Séguin *et al.*, D^3He-proton emission imaging for inertial-confinement-fusion experiments, Rev. Sci. Instrum. **75**, 3520 (2004).

[32] J. A. Frenje *et al.*, Measuring shock-bang timing and ρR evolution of D^3He implosions at OMEGA, Phys. Plasmas **11**, 2798 (2004).

[33] C. Stoeckl, V. Yu. Glebov, S. Roberts, T. C. Sangster, R. A. Lerche, R. L. Griffith, and C. Sorce, Ten-inch manipulator-based neutron temporal diagnostic for cryogenic experiments on OMEGA, Rev. Sci. Instrum. **74**, 1713 (2003).

[34] M. D. Cable, and S. P. Hatchett, Neutron spectra from inertial confinement fusion targets for measurement of fuel areal density and charged particle stopping powers, J. Appl. Phys. **62**, 2233 (1987).

[35] J. T. Larsen, and S. M. Lane, HYADES—A plasma hydrodynamics code for dense plasma studies, J. Quant. Spectrosc. Radiat. Transfer **51**, 179 (1994).

[36] R. Andrae *et al.*, Dos and don'ts of reduced chi-squared, arXiv:1012.3754v1.

[37] T. Nagayama, R. C. Mancini, R. Florido, D. Mayes, R. Tommasini, J. A. Koch, J. A. Delettrez, S. P. Regan, and V. A. Smalyuk, Direct asymmetry measurement of temperature and density spatial distributions in inertial confinement fusion plasmas from pinhole space-resolved spectra, Phys. Plasmas **21**, 050702 (2014).